



Reprint 615

High Resolution Numerical Modelling  
of Windshear Episodes at the Hong Kong International Airport

K.C. Szeto<sup>1</sup> & P.W. Chan

12<sup>th</sup> Conference on Aviation, Range, & Aerospace Meteorology,  
American Meteorological Society, Atlanta, GA, USA,  
29 January - 2 February 2006

<sup>1</sup> *City University of Hong Kong, Hong Kong, China*

K.C. Szeto  
City University of Hong Kong, Hong Kong, China

P.W. Chan \*  
Hong Kong Observatory, Hong Kong, China

### 1. INTRODUCTION

The HKIA is built on a reclaimed island surrounded by the sea on three sides (Figure 1). To the south of it, there is the hilly Lantau Island which has peaks reaching nearly 1000 m AMSL and valleys as low as 300 m. Terrain-induced airflow disturbances (Lau and Shun 2000) and sea breeze (Lee and Shun 2003) are two major causes of low-level windshear at the Hong Kong International Airport (HKIA).

This paper presents the initial results of using a numerical model at a horizontal resolution of 200 m to simulate the typical windshear episodes at HKIA. We employ the Regional Atmospheric Modelling System (RAMS) version 4.4 (Cotton et al. 2001) in the present study. In simulations at sub-kilometre horizontal resolution, RAMS has been found to capture well the terrain-induced circulations in an area of complicated orography (Zhong and Fast 2003). It has also been used extensively in the simulation of sea breeze development (Pielke 2002) and the interaction between sea breeze and the background flow (e.g. Bastin et al. 2005). The model configuration is given in Section 2. Simulation results are discussed in Section 3. Conclusions are given in Section 4.

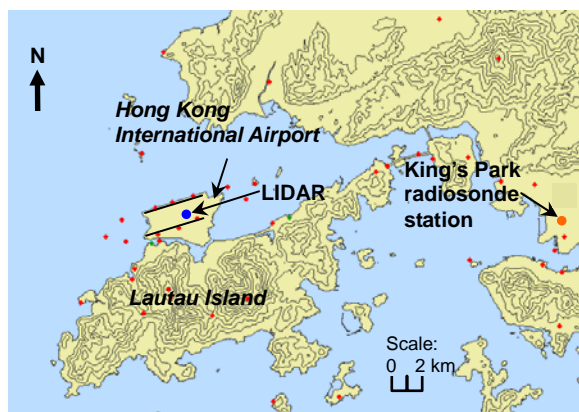


Figure 1 Map of HKIA and the adjacent area (height contours: 100 m). Small red dots represent the ground-based anemometers and weather buoys.

### 2. MODEL CONFIGURATION

We perform RAMS runs in the forecasting mode in three nested grids with grid spacings of 4000, 800 and 200 m. Figure 2 shows the model domains. Two-way interactive nesting is used. Hourly

forecasts from the Regional Spectral Model (RSM) of HKO at 20 km resolution (further information of RSM could be found in Yeung et al. 2005) is employed as the boundary condition for the outermost domain.

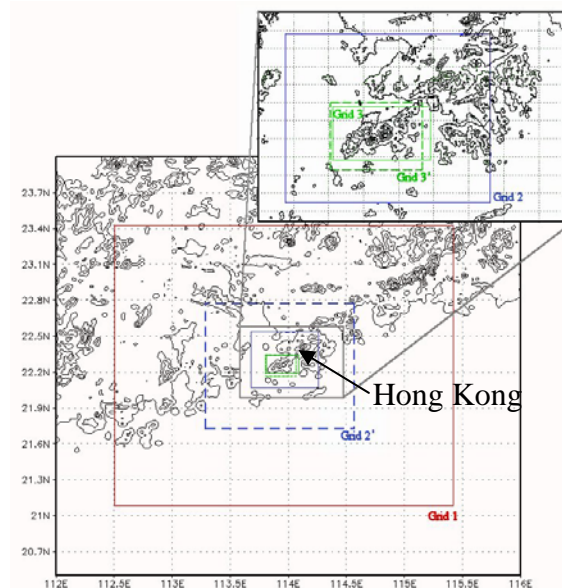


Figure 2 Domains of the nested model grids: solid and broken lines refer to the domains in the forecasting mode (Grids 1, 2 and 3) and the horizontally-homogeneous initialization simulations (Grids 2' and 3') respectively.

### 3. SIMULATION RESULTS

#### 3.1 SEA BREEZE: 6 MARCH 2005

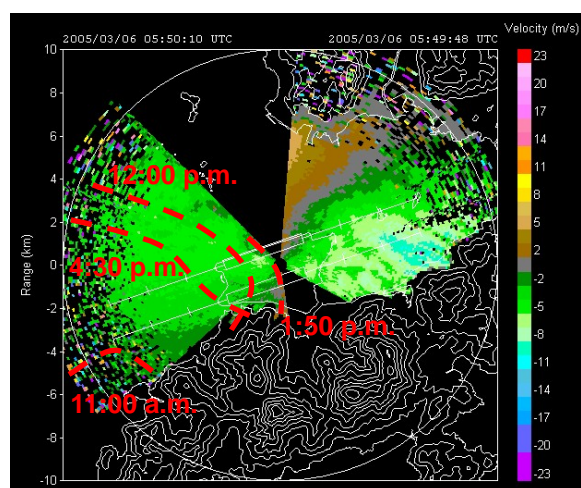
Synoptically, a ridge of high pressure brought an easterly airstream to the south China coast. The troposphere was dry from the radiosonde ascents (not shown) and the sky was nearly cloud-free in the daytime. The temperature at HKIA rose from 12 °C in the early morning to a maximum of about 19 °C in the afternoon, exceeding the sea surface temperature of 15 °C. This favours the occurrence of sea breeze.

As shown in the LIDAR's 0-degree PPI scan imageries, the sea breeze front first appeared at about 11 a.m. (03 UTC, Hong Kong time = UTC + 8 hours) on that day as the westerly sea breeze and the background easterly flow converged over the offshore waters west of Lantau Island (Figure 3(a)). It advanced towards HKIA rather rapidly so that, after about an hour, it had already reached the western part of the airport. It stayed over the airport in the next several hours and retreated to the west in the evening. Six aircraft landing at HKIA from the west reported encounter of significant windshear with headwind gain of 15 – 20 knots at altitude 60 – 90 m between 4:12

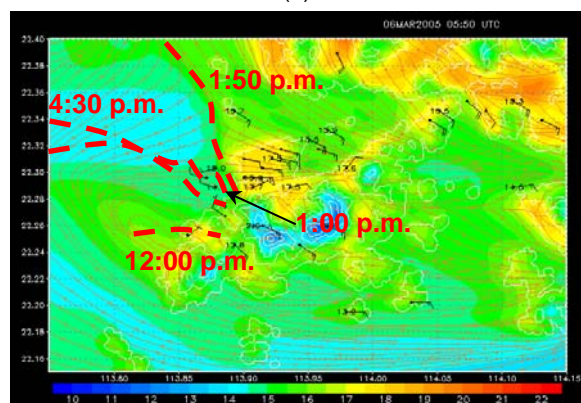
\* Corresponding author address: P.W. Chan, Hong Kong Observatory, 134A Nathan Road, Hong Kong email: [pwchan@hko.gov.hk](mailto:pwchan@hko.gov.hk)

and 4:38 p.m. when the sea breeze front lay across the approach corridor.

The forecasting mode simulation initialized at 8 a.m., 6 March 2005 shows similar evolution of the sea breeze front (Figure 3(b)). Though starting off an hour later compared to the actual observation, the simulated front also appears first to the west of Lantau Island and reaches HKIA in an hour or so. It retreats to the offshore waters west of the airport in the evening. The model simulation essentially reproduces the advancement and retreat of the sea breeze front.



(a)



(b)

Figure 3 LIDAR's radial velocity imagery at 1:50 p.m., 6 March 2005 and the locations of the sea breeze front at different times (a). Streamlines of the wind field at about 50 m AMSL and the surface temperature (colour contours) in the model simulation at the same time as (a) are shown in (b). Marked in (b) as dashed lines are the locations of the sea breeze front from the model result. The surface winds and temperatures predicted by the model are also shown.

### 3.2 EASTERLY WIND CASE: 30 MARCH 2005

In east to southeasterly wind situation, terrain-disrupted airflow with the presence of microscale vortices is occasionally observed to the west of HKIA. The disrupted flow takes the form of decelerated air mass and reversed flow downstream of the hills on Lantau Island. Following the definition of Rotunno et al. (1999), these features could be

regarded as characterizing the presence of mountain wake. Windshear may be encountered as the aircraft flies through the wake (Lau and Shun 2000).

The easterly wind case on 30 March 2005 is studied using horizontally-homogeneous initialization run of RAMS. Between 8 and 11 a.m. on that day, there were altogether 15 aircraft reporting significant windshear on approach from the west. A LIDAR imagery of radial velocity in the period is given in Figure 4, showing the mountain wake west of HKIA.

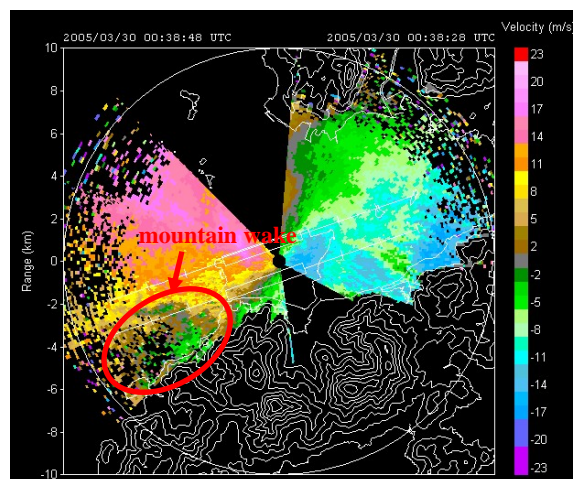


Figure 4 LIDAR's radial velocity imagery at 8:38 a.m., 30 March 2005.

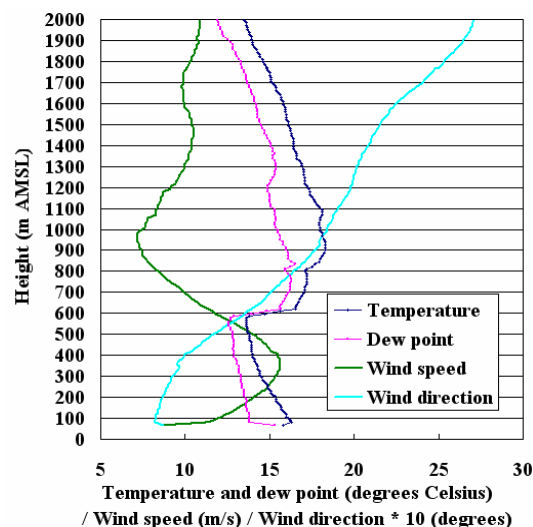


Figure 5 Vertical profiles of temperature, dew point, wind speed and direction obtained from the radiosonde ascent at 8 a.m., 30 March 2005.

Based on the radiosonde measurement (Figure 5) at King's Park (see Figure 1 for its location), the mountain wake occurs in supercritical flow (i.e. Froude number  $> 1$ ). Disruption of supercritical hydrostatic flow by terrain has been studied in the literature using idealized mountain shape. For instance, in Jiang and Smith (2000), an isolated and circular hill was considered and the flow downwind of this hill was shown to depend on two parameters:

- (a) Froude number of the undisturbed flow upstream of the hill,  $F_\infty = U / \sqrt{gD(\Delta\theta/\theta)}$ , where  $U$  is the mean wind speed of the upstream flow,

$g$  the acceleration due to gravity,  $D$  the altitude of the inversion,  $\Delta\theta$  the magnitude (in potential temperature) of the inversion and  $\theta$  the mean potential temperature of the inversion layer;

- (b) dimensionless mountain height,  $M=H/D$ , where  $H$  is the characteristic mountain height.

A regime diagram was also constructed in Jiang and Smith (2000) to delineate the flow patterns in the  $F_\infty \times M$  space. Even the flow considered here is not purely hydrostatic, the wake of the Lantau terrain is studied here to establish its relationship with the wind speed and temperature inversion in the upstream flow and to see whether a similar regime diagram could be obtained.

A control run is first performed by initializing RAMS homogeneously with the vertical profiles given in Figure 5. The simulation result is shown in Figure 6. The location of the mountain wake is consistent with the LIDAR observation.

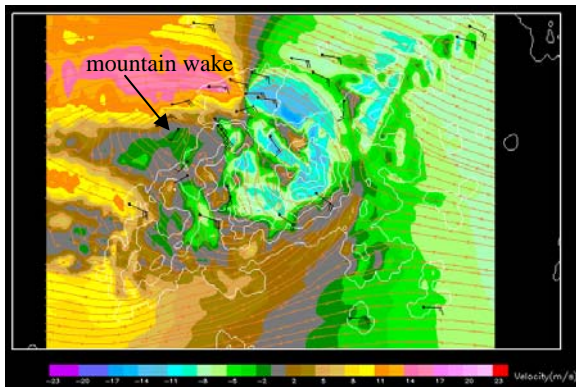


Figure 6 Surface (wind barbs) and 50-m winds (streamlines and velocities resolved along the LIDAR's radials) at the time of the largest mountain wake west of HKIA in the horizontally-homogeneous initialization run based on the vertical profiles in Figure 5

Category	Parameter			
	Max speed of the jet (m/s)	$U$ (m/s)	$\Delta\theta$ (K)	$D$ (m)
Small	11	9.5-10.2	1.0	300
Original	15.6	10.3-13.0	3.4	600
Large	20	15.0-17.0	4.5	900

Table 1 The values of  $U$ ,  $\Delta\theta$  and  $D$  in the three categories

The vertical profiles in Figure 5 are then modified by varying three parameters: maximum wind speed of the boundary layer jet, magnitude of the temperature inversion and height of the inversion. The mean wind speed in the inversion layer (as input to  $F_\infty$ ) is changed at the same time, depending on the values of the maximum wind speed of the jet as well as the inversion's height. Moreover, it seems from Figure 5 that the temperature inversion and the jet are coupled features in the boundary layer and thus their heights are not varied independently in this experiment. Instead, the inversion's height is changed, and the height of the jet is modified in proportion. Each of the three parameters is varied according to three "categories": the "original" magnitude range, a range of "small" magnitude, and a range of "large" magnitude, as given in Table 1. So

in total, there are 27 different combinations of the parameters for conducting the homogeneous initialization runs.

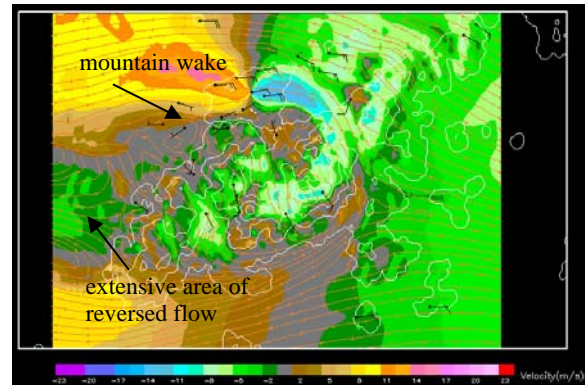


Figure 7 Same as Figure 6, but for small  $U$ , large  $\Delta\theta$  and small  $D$

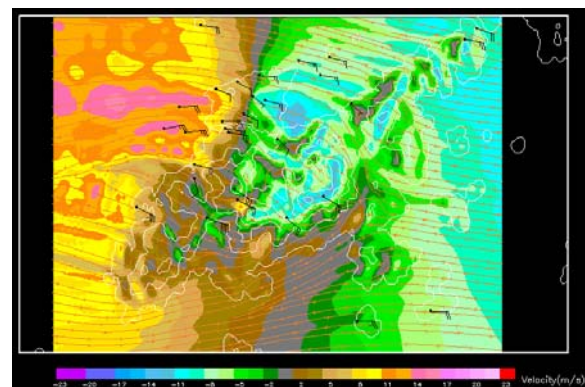


Figure 8 Same as Figure 6, but for large  $U$ , small  $\Delta\theta$  and large  $D$

It turns out that most of the parameter combinations produce a mountain wake to the west of HKIA, though with different sizes. In some "extreme" combinations in which the inversion is low and strong and the jet's speed is small, there is an extended area of reversed flow (against the prevailing easterly) to the west of Lantau Island (Figure 7). On the other hand, if the inversion is high and weak, the air flows over the Lantau terrain readily and no mountain wake is discernable to the west of HKIA (Figure 8).

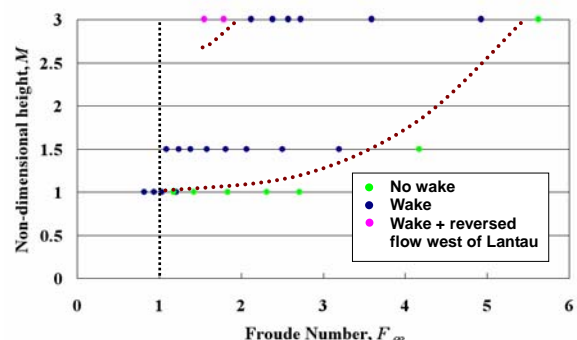


Figure 9 Regime diagram ( $M \times F_\infty$ ) for Lantau Island simulations and regime boundaries (brown dotted lines).

The simulation results are summarized in the form of a regime diagram (Figure 9) with two controlling parameters: Froude number  $F_\infty$  and non-dimensional mountain height  $M$  (the characteristic

mountain height  $H$  is taken to be 900 m). Similar to the results in Jiang and Smith (2000), it seems that there are two regime boundaries in the supercritical flow. Of course, the exact locations of the regime boundaries in the present study and those in Jiang and Smith (2000) could be different because a more realistic and complex terrain and non-hydrostatic flow is considered here. Nonetheless, the present results suggest that in general distinctive flow regimes may exist for terrain-disrupted airflow, irrespective of the geometry of the terrain. The regime diagram like Figure 9 is useful in windshear alerting by assessing the chance of the occurrence of the mountain wake.

#### 4. CONCLUSIONS

Numerical simulations at a horizontal resolution down to 200 m were performed using RAMS to study some typical cases of terrain-disrupted airflow and sea breeze at HKIA, which are the two major causes of low-level windshear to the aircraft. The simulation results reproduced the salient features of the airflow in these cases, such as advancement and retreat of the sea breeze front and mountain wake to the west of HKIA.

Homogeneous initialization simulations, despite using idealized inputs in comparison to the forecasting mode runs, gave useful insights into the meteorological factors relating to the mountain wake west of HKIA. A regime diagram in non-dimensional mountain height and Froude number was constructed. It could be useful for windshear alerting by assessing the chance of occurrence of mountain wake.

#### Acknowledgement

The research work in this paper was carried out by Mr. K.C. Szeto of City University of Hong Kong (CityU) during his attachment to HKO in 2005 under the Co-operative Education Scheme between HKO and CityU.

#### References

- Bastin, S., P. Drobinski, O. Bock, J.L. Caccia, B. Campistron, C. Champollion, A.M. Dabas, P. Delville, V. Guénard, F. Masson, O. Reitebuch and C. Werner, 2005: On the interaction between sea breeze and summer Mistral at the exit of the Rhône valley during the ESCOMPTE experiment. *Croatian Meteorological Journal*, **40**, 128-131.
- Cotton, W.R., R.A. Pielke Sr., R.L. Walko, G.E. Liston, C. Tremback, H. Jiang, R.L. McAnelly, J.Y. Harrington, M.E. Nicholls, G.G. Carrio and J.P. McFadden, 2003: RAMS 2001: Current status and future directions. *Meteor. Atmos. Phys.*, **82**, 5-29.
- Jiang, Q., and R. B. Smith, 2000: V-waves, bow shocks and wakes in supercritical hydrostatic flow. *J. Fluid Mech.*, **406**, 27-53.
- Lau, S.Y., and C.M. Shun, 2000: Observation of terrain-induced windshear around Hong Kong International Airport under stably stratified conditions. *9<sup>th</sup> Conference on Mountain Meteorology*, American Meteorological Society, Colorado.
- Lee, O., and C.M. Shun, 2003: Observation of sea breeze interactions at and near Hong Kong International Airport. *Meteor. Appl.*, **10**, 1-9.
- Pielke, R.A., 2002: *Mesoscale Meteorological Modelling*. 2d ed. Academic Press, 676 pp.
- Rotunno, R., V. Grubiši, and P. K. Smolarkievicz, 1999: Vorticity and potential vorticity in mountain wakes. *J. Atmos. Sci.*, **56**, 2796-2810.
- Yeung, L.H.Y., P.K.Y. Chan and E.S.T. Lai, 2005: Impact of radar rainfall data assimilation on short-range quantitative precipitation forecasts using four-dimensional variational analysis technique. *32<sup>nd</sup> Conference on Radar Meteorology*, American Meteorological Society, New Mexico (on-line proceedings).
- Zhong, S., and J.D. Fast, 2003: An evaluation of the MM5, RAMS, and Meso-Eta models at subkilometer resolution using VTMX field campaign data in the Salt Lake Valley. *Mon. Wea. Rev.*, **131**, 1301-1322.